THE JOURNAL OF BIOLOGICAL CHEMISTRY VOL. 283, NO. 49, pp. 34414–34422, December 5, 2008

Nanoscale Increases in CD2-CD48-mediated Intermembrane Spacing Decrease Adhesion and Reorganize the Immunological Synapse*[S]

Received for publication, June 23, 2008, and in revised form, August 28, 2008 Published, JBC Papers in Press, September 30, 2008, DOI 10.1074/jbc.M804756200

Oren Milstein[‡§], Su-Yi Tseng[‡], Toby Starr[‡], Jaime Llodra[¶], Andrea Nans[¶], Mengling Liu[‖], Martin K. Wild[**], P. Anton van der Merwe[‡‡], David L. Stokes[¶], Yair Reisner[§], and Michael L. Dustin[‡1]

From the Programs in [‡]Molecular Pathogenesis and [¶]Structural Biology, Helen and Martin Kimmel Center for Biology and Medicine of the Skirball Institute and New York University School of Medicine, New York, New York 10016, the [‖]Division of Biostatistics, New York University Cancer Institute, New York, New York 10016, the [§]Department of Immunology, Weizmann Institute of Science, Rehovot 76100, Israel, the [**]Max Planck Institute of Molecular Medicine, 48149 Muenster, Germany, and the [‡‡]Sir William Dunn School of Pathology, Oxford University, South Parks Road, Oxford OX1 3RE, United Kingdom

The relationship between intermembrane spacing, adhesion efficiency, and lateral organization of adhesion receptors has not been established for any adhesion system. We have utilized the CD2 ligand CD48 with two (wild type CD48 (CD48-WT)), four (CD48-CD2), or five (CD48-CD22) Ig-like domains. CD48-WT was 10-fold more efficient in mediating adhesion than CD48-CD2 or CD48-CD22. Electron tomography of contact areas with planar bilayers demonstrated average intermembrane spacing of 12.8 nm with CD48-WT, 14.7 nm with CD48-CD2, and 15.6 nm with CD48-CD22. Both CD48-CD2 and CD48-CD22 chimeras segregated completely from CD48-WT in mixed contact areas. In contrast, CD48-CD2 and CD48-CD22 co-localized when mixed contacts were formed. Confocal imaging of immunological synapses formed between primary T lymphocytes and Chinese hamster ovary cells presenting major histocompatibility complex-peptide complexes, and different forms of CD48 demonstrated that CD48-CD2 and CD48-CD22 induce an eccentric CD2/T cell antigen receptor cluster. We propose that this reorganization of the immunological synapse sequesters the T cell antigen receptor in a location where it cannot interact with its ligand and dramatically reduces T cell sensitivity.

T cell activation requires interactions of T cell antigen receptors (TCRs)[2] with peptide-presenting major histocompatibility complexes (MHCp), which are anchored to the plasma membrane of the T cell and antigen-presenting cells, respectively (1, 2). Adhesion molecule pairs facilitate this process by physically holding the cells together and providing additional signals that are integrated by the T cell (3, 4). Adhesion molecules that participate in T cell activation can be categorized into at least two groups: the integrin family adhesion molecules that include lymphocyte function-associated antigen (LFA)-1 on T cells, which interacts with intercellular adhesion molecule (ICAM)-1 on antigen-presenting cells, and the small immunoglobulin superfamily molecules like CD2 on T cells, which interacts with CD48 on the surface of antigen-presenting cells (3, 5).

Adhesion molecules and TCR are organized in an immunological synapse (IS) (6, 7). Supported planar bilayers containing ICAM-1 and MHCp reconstitute formation of the IS (8). This model IS is characterized by a bull's eye-like configuration of a central supramolecular activation complex (cSMAC) enriched in TCR, a peripheral supramolecular activation complex enriched in LFA-1, and a distal supramolecular activation complex enriched in CD45 and F-actin (9). The distal supramolecular activation complex is essentially a radial lamellipodium (10) that is the site of nucleation of segregated TCR and LFA-1 microclusters that are transported by centripetal actin flow to the cSMAC via the peripheral supramolecular activation complex (11, 12). Signaling in TCR microclusters takes place during this transport process, and signaling is inactivated in the cSMAC (11, 13, 14). The mechanism by which TCR and LFA-1 initially segregate is not known.

Springer (3) speculated that receptor size could lead to segregation of LFA-1 from TCR in a contact area. LFA-1, like other integrins, is a large noncovalent transmembrane heterodimer and undergoes dramatic conformational changes leading to extension of ~28 nm from the membrane surface (15). ICAM-1 is also a relatively long molecule predicted to project ~18 nm from the surface (16). The TCR and MHCp project about 7.5 nm from the surface each and are predicted to interact across an intermembrane distance of ~13 nm (1). The interaction of CD2 with CD48 generates a complex that is also ~13 nm long,

* This work was supported, in whole or in part, by National Institutes of Health Grants AI43542 (to M. L. D.), GM071044 (to D. L. S.), and P30 CA016087 (to M. L.). This work was also supported by European Molecular Biology Organization Fellowship ASTF.49.00-05 (to O. M.) and Leukemia and Lymphoma Society Fellowship 5456-04 (to S. Y. T.). The costs of publication of this article were defrayed in part by the payment of page charges. This article must therefore be hereby marked "*advertisement*" in accordance with 18 U.S.C. Section 1734 solely to indicate this fact.

[S] The on-line version of this article (available at http://www.jbc.org) contains TIFF files containing the raw data for the representative three-dimensional data sets in Figs. 5 and 6. The files are are named based on the figure component and channel. These data can be inspected with image processing software, such as ImageJ (available on the World Wide Web).

[1] To whom correspondence should be addressed: Program in Molecular Pathogenesis, New York University School of Medicine, 540 1st Ave., New York, NY 10016. Tel.: 212-263-3207; Fax: 212-263-5711; E-mail: dustin@saturn.med.nyu.edu.

[2] The abbreviations used are: TCR, T cell receptor; cSMAC, central supramolecular activation cluster; ICAM, intercellular adhesion molecule; IS, immunological synapse; LFA, lymphocyte function-associated antigen; MCC, moth cytochrome *c*; MHC, major histocompatibility complex; MHCp, MHC-peptide; CD48-WT, wild type CD48; FITC, fluorescein isothiocyanate; APC, antigen-presenting cell; CHO, Chinese hamster ovary.

as was first suggested by mutagenesis and modeling studies (17) and later confirmed in structural studies (18). The CD2-CD58 interaction segregates from the LFA-1-ICAM-1 interaction in sites of adhesion, but it is not clear if this is due to size differences or to differential membrane and cytoskeletal interactions (7). The manner in which apparent molecular size, actual intermembrane spacing, and lateral organization are related is not clear. Linear assumptions can be misleading, based on electron microscopy tomography studies of desmosomal cadherins, in which significant bending of molecules is observed (19, 20).

A dual role of both signaling and adhesion has been attributed to the CD2-CD48 interaction. CD2 cross-linking can lead to T cell activation in a manner dependent upon co-expression of the TCR (21). CD2 has a large highly conserved cytoplasmic domain that mediates activation of the Src family kinase Fyn (22). CD2 is recruited to sites of TCR engagement even in the absence of ligand (23, 24).

Wild type CD48 (CD48-WT) has two Ig-like domains and enhances T cell activation when present on APCs. Chimeric CD48, which are identical except for the addition of two (CD48-CD2) or three (CD48-CD22) additional Ig-like domains, both inhibit T cell activation while mediating adhesion (25). The impact of elongated forms of CD48 on adhesion efficiency, the intermembrane gap, organization of contact area, or the structure of the IS have not been determined. Similar constructs that added four Ig-like domains to MHC molecules, adding a structural length of 14–16 nm, only increased the average intermembrane separation by 4.7 nm (26).

In this study we performed a detailed comparison of CD48-WT, CD48-CD2, and CD48-CD22 for efficiency of cell adhesion, intermembrane separation, lateral segregation, and organization of the IS. Utilizing the planar bilayer system, we were able to examine the effects of ligand elongation directly. Increasing the length of CD48 decreased its efficiency as an adhesion system by 10-fold and increased the intermembrane separation by ~1 nm/Ig-like domain. There were two outcomes observed in mixed systems: interference, in which the presence of one CD2 ligand dramatically decreased or eliminated engagement by the other, and segregation, in which each system interacted in adjacent micrometer scale membrane domains. Differences of 2–3 Ig-like domains led to interference and segregation, whereas differences of 1 Ig domain permitted co-localization. Expression of CD48-CD2 or CD48-CD22 on the antigen-presenting cell attenuated naive T cell detection of antigen and disrupted symmetry of the immunological synapse.

EXPERIMENTAL PROCEDURES

Cells and Constructs—CHO cell lines expressing recombinant CD48-WT, CD48-CD2, and CD48-CD22 were previously described (25).

Protein Purification—CD48 forms were purified from detergent lysates of CHO cells using OX78-Sepharose, as previously described (27).

Mice and T Cell Activation—Mice were housed in accordance with Institutional Animal Care and Use Committee guidelines. Splenocytes from B10.A 5C.C7 TCR mice were activated by the addition of moth cytochrome *c* peptide (residues 88–103) ANERADLIAYLKQATK to prepare T cell blasts as previously described (8).

T Cell Proliferation Assay and Fluorescence-activated Cell Sorting Analysis—Proliferation assays by carboxyfluorescein succinimidyl ester dilution were performed as previously described (28). Briefly, naive $CD4^+$ T cells were purified from 5C.C7 mice by enrichment using magnetic beads (Miltenyi, Auburn, CA). The cells were labeled with 2 μM carboxyfluorescein succinimidyl ester for 20 min (Invitrogen). After washing, the cells were placed in complete medium and cultured with CHO cells. Proliferation was determined based on the percentage of cells that had divided at least once.

Fluorescence Microscopy and Image Analysis—Moth cytochrome *c* (MCC) peptide-pulsed CHO cells were allowed to grow overnight in 8-well Lab-Tek chambered 0.17 mm thickness borosilicate coverglass systems (Nalge-Nunc, Rochester, NY), after which they were cultured with T cells for 30 min at 37 °C and fixed with 2% methanol-free formaldehyde/phosphate-buffered saline. Antibody staining was performed as previously described, and images were taken with a LSM 510 confocal microscope (Carl Zeiss, Thornwood, NY) (28). Image stacks consisted of 8–22 planes spaced at a 0.48-μm interval to include the IS. These image stacks were rendered in three dimensions and were analyzed using Volocity software (Improvision, Lexington, MA). Two-dimensional projections from rendered three-dimensional data sets rotated into the en face and side orientations were generated in Volocity. CD2 and TCR were considered as accumulated in clusters only when 1.5 times brighter than the surrounding membrane.

Electron Tomography—Cells were fixed by the addition of a 1% glutaraldehyde, 3% formaldehyde, and 0.3% tannic acid mixture in 0.1 M cacodylate buffer, pH 7.4, and then 1% osmium tetroxide solution for 1 h at room temperature. Samples on planar bilayers were embedded and sectioned as described (29).

Tilt series for electron tomography were recorded at ×20,000 magnification with a pixel size of 0.89 nm using an electron microscope operating at 200 kV (CM200 Philips Electron Optics, Eindhoven, The Netherlands) and a 1024 × 1024 CCD camera (Gatan Corp., Pleasanton, CA). Each tilt series ranged from −60 to +60° with images recorded at 2° intervals. Individual images were aligned, and tomograms were generated using a marker-free algorithm developed by Winkler and Taylor (30). Distances between the middle of the supported bilayer and the middle of the lymphocyte plasma membrane were measured in individual tomographic slices by drawing a rectangle at well preserved contact areas and calculating the width using ImageJ. This minimizes error in estimating the distance perpendicular to the apposed bilayers.

Antibodies—Fluorescein isothiocyanate (FITC)-anti-I-E^k (14-4-4s clone; BD Pharmingen), Alexa 488-anti-CD48 (OX78 clone) (5), FITC-anti-CD2 (clone T11; Beckman Coulter), and FITC-anti-mouse CD22 (clone Cy34.1; BD Pharmingen) were used for flow microfluorimetry. Calibration was performed with FITC standard beads (Bangs Laboratories, Fishers, IN). Alexa 488-anti-CD48 (OX78 clone), Alexa 546-anti-mouse CD2 (clone RM2–5; eBioscience), and Cy5-anti-TCR (clone H57) were used in imaging. Anti-hamster ICAM-1-blocking

antibody (clone J5-3F9) was kindly provided by V. Kuchroo (31).

Planar Bilayer Studies—CD48 was purified by immunoaffinity chromatography using OX78 antibody, labeled with amine-reactive fluorescent dyes, and incorporated into unilamellar liposomes with a final concentration of 0.4 mM egg phosphatidylcholine (Avanti Polar Lipids, Alabaster, AL). The density of CD48 in the bilayers was determined by depositing bilayers on 5-μm glass beads, reacting these with saturating concentrations of FITC-OX78, and analyzing fluorescence on a flow microfluorimeter using FITC standard beads (Bangs Laboratories) for calibration. Supported planar bilayers were prepared in a parallel plate flow cell (Bioptechs, Butler, PA). Imaging was performed on a wide field fluorescence microscope with an Orca ER camera (Hammamatsu, Bridgewater, NJ) using IP Lab software (BD Bioscience and Bioimaging) (27, 32).

Statistical Analysis—Adhesion data were analyzed with a Wilcoxon rank sum test. Electron microscopy results were analyzed using a *t* test. IS patterns were analyzed by analysis of variance. Provided a significant difference existed, Dunnett's *post hoc* comparison was used to compare individual cell lines to the control line, and differences were considered significant when p was less than 0.05 (SAS Institute).

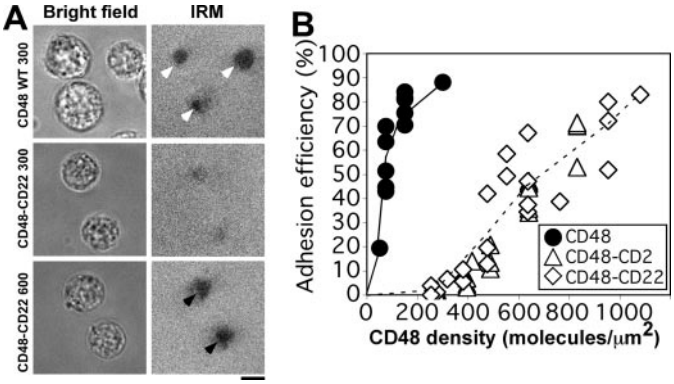

FIGURE 1. **Adhesive efficiency of CD48-WT and CD48-CD22.** *A*, *images* of murine T cells adhering to bilayers. Bright field and interference reflection microscopy are shown for CD48-WT and CD48-CD22 at 300 molecules/μm^2 and for CD48-CD22 at 600 molecules/μm^2. All experiments were repeated at least three times. *Scale bar*, 5 μm. *B*, percentage adhesion was determined as a function of Cy5-CD48-WT (*circles*), Cy5-CD48-CD2 (*triangles*), and Cy3-CD48-CD22 (*diamonds*) density at 24 °C for 1 h based on interference reflection microscopy without application of any external force.

RESULTS

Increasing CD48 Length Decreases Adhesion Efficiency—To directly evaluate the effect of increasing CD48 length on adhesion, we used supported planar bilayers containing identically purified and fluorescently labeled CD48-WT, CD48-CD2, or CD48-CD22 at different densities and compared the adhesion of mouse T cell blasts by counting contact areas by interference reflection microscopy over a range of densities (25–1000 blasts/μm^2). T cells were allowed to interact with bilayers for 1 h at 24 °C, which is sufficient time for adhesion by all forms to reach equilibrium. CD48-WT mediated ~50% adhesion at 50 molecules/μm^2, whereas CD48-CD2 or CD48-CD22 required 600 molecules/μm^2 to mediate ~50% adhesion (Fig. 1*A*). The difference in adhesion between CD48-WT and CD48-CD2 or CD48-CD22 was significant at $p = 0.00071$ and 0.0021, respectively. The difference between CD48-CD2 and CD48-CD22 was not significant, with $p = 0.75$. Interference reflection microscopy revealed similar sized contact areas for CD48-WT and CD48-CD22 (Fig. 1*B*). These findings suggest that the CD48-WT is ~10-fold more efficient at mediating adhesion than either extended form of CD48.

Electron Tomography on Contact Areas Mediated by CD48-WT or Elongated Forms of CD48—The impact of changing the size of CD48 on intermembrane spacing was examined by electron tomography. Mouse T cell blasts were allowed to adhere to planar bilayers containing either 75 molecules/μm^2 of CD48-WT or 600 molecules/μm^2 of CD48-CD2 or CD48-CD22 to ensure similar adhesion. The cells were fixed after 1 h and subjected to electron tomography and three-dimensional reconstruction for measurements of the intermembrane distance perpendicular to the planar bilayer. Representative projections for CD48-WT and CD48-CD22 are shown in Fig. 2*A*. Although linear assumptions would lead to a prediction of 4 nm/Ig-like domain, the real increase in intermembrane spacing was closer to 1 nm/Ig-like domain, based on intermembrane distances of 12.8 ± 1.4 nm for CD48-WT, 14.7 ± 1.2 for CD48-CD2, and 15.6 ± 1.4 nm for CD48-CD22 (Fig. 2*B*). Differences between groups were statistically significant at $p < 0.0001$. Similar results were obtained previously in cell-cell contacts with extended TCR-MHCp interactions (26).

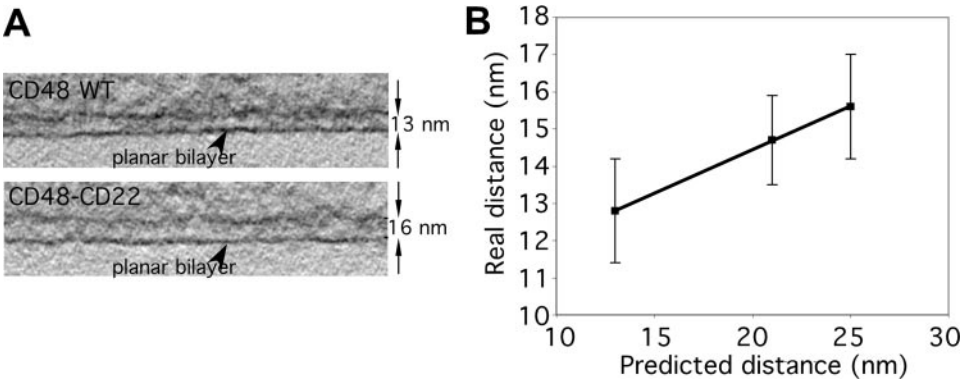

FIGURE 2. **Analysis of intermembrane spacing by electron tomography.** *A*, electron tomography *images* of T cell adhering to planar bilayer with an indication of average intermembrane distance. *B*, mean intermembrane distance. For CD48-WT, $n = 84$ measurements on 12 cells; for CD48-CD2, $n = 108$ measurements on 8 cells; for CD48-CD22, $n = 63$ measurements on seven cells. All values are significantly different at $p < 0.0001$. Measurements within a single cell contact had errors (4.7, 5.3, and 5.8% for CD48-WT, CD48-CD2, and CD48-CD22, respectively) that were smaller than measurements between different cells (8.8, 6.1, and 6.6% for CD48-WT, CD48-CD2, and CD48-CD22, respectively).

Lateral Segregation Based on Differences in Intermembrane Distance Using the Same Receptor—We next asked whether any lateral segregation of receptor-ligand interactions results from the difference in intermembrane spacing noted above. Murine T cell blasts were allowed to adhere to bilayers containing Cy5-CD48-WT, Cy3-CD48-CD2, and

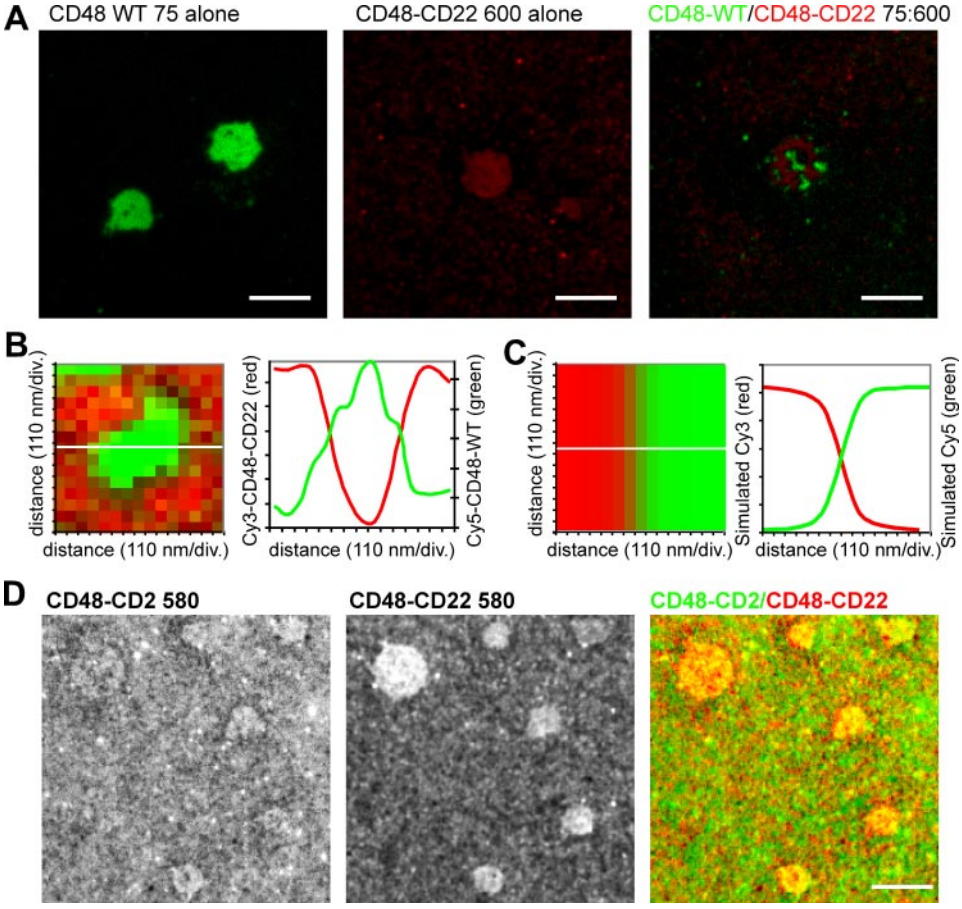

FIGURE 3. **Segregation of CD2/CD48-WT and CD2/CD48-CD22 interactions in the same contact area.** *A*, mouse T cells adhering to 75 molecules/μm^2 Cy5-CD48-WT, 600 molecules/μm^2 Cy3-CD48-CD22, or the combined bilayer of 75 molecules/μm^2 Cy5-CD48-WT and 600 molecules/μm^2 Cy3-CD48-CD22. Note that these are each from different bilayers and fields. The *images* show molecular densities as *lightest* to *darkest colors*, corresponding to a range of 75–275 molecules/μm^2 for CD48-WT (*green*) and 600–800 molecules/μm^2 for CD48-CD22 (*red*). The experiment was repeated five times. *Scale bar*, 5 μm. *B*, details of two regions from mixed contact areas showing 110-nm pixels and line scan (*white lines*). Similar results were obtained from 10 contact areas. *C*, experimental point spread function for Cy3 (*red*) and Cy5 (*green*) channels was used to simulate adjacent adhesion domains with a separation of 110 nm. Note the similarity of the line scan profile between the experimental data and the simulation. *D*, mixed contact areas formed with bilayers containing Cy5-CD48-CD2 and Cy3-CD48-CD22 (each at 580 molecules/μm^2). The *images* are of the *same* field with the Cy-5-CD48-CD2, Cy3-CD48-CD22, and merged channels shown (*left* to *right*). This contact is representative of 84% of 148 contacts examined. The remaining contacts had CD48-CD22 only (12%) or CD48-CD2 only (4%). *Scale bars*, 5 μm.

Cy3- or Cy5-CD48-CD22 or each pairwise combination. In all bilayers, the molecular density of the respective CD48 form was adjusted to give an equal percentage of adhesion, 75 molecules/μm^2 for CD48-WT and 600 molecules/μm^2 for CD48-CD2 or CD48-CD22. The interaction of CD2 with CD48 was visualized as fluorescence accumulation. When T cells interacted with bilayers carrying CD48-WT or CD48-CD22 separately, we observed a homogeneous accumulation of the respective CD48 throughout the entire area of contact, with higher levels of accumulation in CD48-WT than CD48-CD22 (Fig. 3*A*). When T cells interacted with bilayers carrying mixtures of CD48-WT with CD48-CD22 at densities giving equal adhesion, they were co-engaged in the same contact area in 63% of contacts formed (n = 130; Fig. 3*A*). Under these conditions, the interactions were always laterally segregated. When the density of CD48-WT was increased by 20%, the proportion of contact areas that accumulated CD48-WT without CD48-CD22 increased to 77% at the expense of the mixed contacts, which were reduced to 20% (n = 63). Conversely, when the density of CD48-WT was decreased by 20%, the proportion of contacts that accumulated CD48-CD22 without CD48-WT increased to 90%, and no mixed contacts were observed (n = 61). Thus, mixed contact areas are formed in a relatively narrow range of CD48-WT/CD48-CD22 ratios.

Analysis of the density of CD48-WT, CD48-CD2, and CD48-CD22 accumulation in single component contact areas showed that each alone accumulated to similar levels with 293 molecules/μm^2 (n = 13), 258 molecules/μm^2 (n = 41), and 218 molecules/μm^2 (n = 133), respectively. More detailed analysis of the segregated domains in mixed contacts revealed that the density of ligand accumulation in the mixed contacts was 110% of the corresponding single component contacts for CD48-CD22 (n = 5) but was 37% of the corresponding single component contacts for CD48-WT (n = 5). Plotting the density of accumulated ligands along a line running through the contact shows that the transitions between domains were sharp, often taking place in an interval of 110-nm pixels (Fig. 3*B*). Indeed, comparison with simulations generated using the point spread function of the imaging system (Fig. 3*C*) shows that the actual transitions between domains are best reconstructed by a gap of 110 nm between areas of Cy3 and Cy5 fluorescence.

When CD48-CD2 and CD48-CD22 were combined in a bilayer at equal ratios at 580 molecules/μm^2 each, which provides an identical adhesion level, the CD48-CD22 interaction was more abundant than the CD48-CD2 interactions; 84% of contact areas displayed spatial overlap of accumulated ligands, and none displayed segregation (n = 148) (Fig. 3*D*). When combined in the same bilayers, the density of accumulated CD48-CD2 decreased by 18-fold compared with the single component system, whereas the density of accumulated CD48-CD22 decreased by only 1.4-fold based on measurements on 21 randomly selected contacts. This was surprising, because we anticipated that these constructs would compete equally based on similar adhesion efficiency and that they might segregate based on the size difference. The results demonstrate that a single Ig domain difference is not sufficient to induce segregation and that for unknown reasons the larger CD48-CD22 molecules

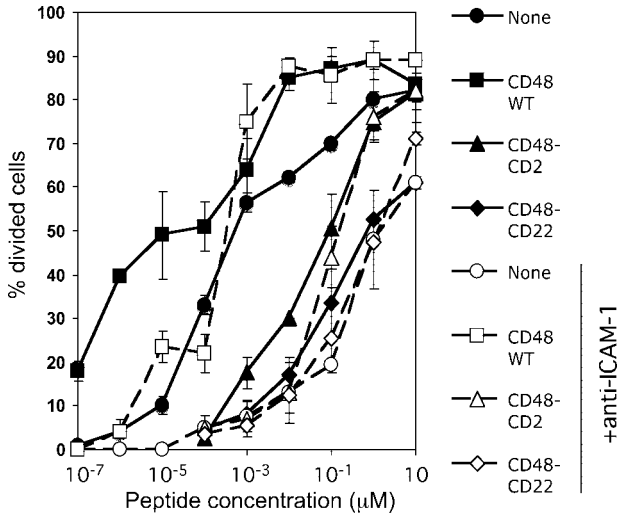

FIGURE 4. **Elongated forms of CD48 inhibit T cell activation.** Dependence of T cell proliferation on CD48 size. Carboxyfluorescein succinimidyl ester-labeled 5C.C7 T cells were added to CD48-negative, CD48-WT, CD48-CD2, or CD48-CD22 I-E^{k+} CHO transfectants pulsed with 10^{-7} to 10 μM MCC peptide with or without anti-ICAM-1 antibody and analyzed by flow cytometry at 72 h. Below 10^{-5} μM peptide, proliferation of T cells being stimulated by elongated forms or ICAM-1-blocked CD48-negative CHOs was consistently null. Data shown are representative of three independent experiments and were obtained as described in *B*. The *error bars* represent S.D. from triplicate data sets.

have an advantage over the CD48-CD2 molecules in direct competition for binding to cell surface CD2.

Impact of the Different CD48 Forms on Primary T Cells—Wild *et al.* (25) previously demonstrated that extended forms of CD48 inhibit recognition of antigen by T cell hybridomas. Since T cell hybridomas do not form well organized ISs, we needed to determine the functional effects of extended forms of CD48 on primary T cells, which form well organized IS. The functional significance of varying the length of the CD2-ligand interaction was studied using primary 5C.C7 T cells as responders and a series of I-E^k-expressing CHO cell transfectants as APCs (25). 5C.C7 T cells are activated by a peptide derived from MCC 88–103 in the context of the MHC II molecule I-E^k. Each CHO cell transfectant stably expresses I-E^k and one of three forms of CD48 at 2×10^6 molecules/cell. The surface area of osmotically swollen CHO cells was 1424 μm^2 (data not shown). Thus, the approximate density of bound OX78 on the surface of the CHO cells is 1400 molecules/μm^2. This density should be adequate to mediate maximal adhesion for all forms of CD48, based on the supported planar bilayer data.

The effect of CD48 length on T cell activation was assessed by carboxyfluorescein succinimidyl ester dilution in naive primary T cells. Naive T cells were isolated from lymph nodes of 5C.C7 $RAG^{-/-}$ mice, and $CD4^+$ T cells were purified. T cells were stained with carboxyfluorescein succinimidyl ester and cultured with CD48 null-, CD48-WT-, CD48-CD2-, or CD48-CD22-transfected I-E^{k+} CHO cells in the presence of different concentrations of MCC peptide, and the percentage of divided cells was used to assess proliferation (Fig. 4, *filled symbols*). CHO APCs transfected with the CD48-WT induced markedly more proliferation than CD48 null CHO cells. This enhancement was evident throughout the range of peptide concentrations used but was most striking at lower peptide concentrations. Conversely, I-E^k CHO cells transfected with the elongated CD48 forms inhibited proliferation compared with CD48-negative CHO cells. The longer CD48-CD22 was a more potent inhibitor than CD48-CD2. This inhibition was partially overcome at high peptide concentration, which would allow analysis of IS formation.

The major endogenous costimulatory molecule expressed on CHO cells is ICAM-1 (31). To focus on CD48-mediated effects, we repeated the proliferation experiments with anti-hamster ICAM-1-blocking monoclonal antibody (Fig. 4, *open symbols*). We found that in the absence of LFA-1-ICAM-1 interactions, CD48-WT was much less effective at promoting highly sensitive T cell activation. In the absence of the LFA-1-ICAM-1 pathway, the CD48-CD2-transfected CHO cells performed significantly better than the CD48 null CHO cells, and CD48-CD22 was no longer inhibitory. In the absence of LFA-1-ICAM-1-dependent adhesion, the elongated forms of CD48 may serve as adhesion ligands and thus take on a more positive role. Nonetheless, these results suggest that elongated forms of CD48 are most inhibitory when in the context of an ICAM-1- and agonist MHCp-dependent IS.

CD48 Length and CD2 Accumulation Pattern; CD48 Length Affects Distribution—Relating molecular patterns in the IS to the functional changes might help to clarify the significance of molecular patterns and provide insight into the mechanism of inhibition by elongated CD48 molecules. CD2 molecules typically accumulate near the cSMAC (8, 33), which may reflect the convergence of active TCR microclusters. To test T cell-APC IS formation, naive 5C.C7 T cells from mice were seeded on non-confluent monolayers of the different I-E^k CHO cell transfectants that had been preincubated in the presence of 10 μM MCC peptide. After 30 min, cells were washed, fixed, and stained for CD2 and CD48. Confocal imaging was performed, and image stacks were rendered in three dimensions to allow visualization of the entire IS from different points of view. The rendering process involved interpolation to fill in missing information between images. After defining features in the rendered images, we reexamined the raw data to make sure that molecular features scored in the rendered images were clearly present in the raw data and thus could not be artifacts of the three-dimensional rendering process (see supplemental material). These images revealed that when T cells were conjugated to CHO cells transfected with CD48-WT, the pattern in 66% of conjugates was for CD2 to aggregate centrally (Fig. 5, *A* and *D*). However, among T cells conjugated to APCs transfected with CD48-CD2 or CD48-CD22, only 20 and 12% (both significantly less than wild type; $p < 0.0001$) had accumulated CD2 in the center of contact, respectively (Fig. 5, *B–D*). Instead, the pattern in 42% of conjugates with CD48-CD2 CHOs and 59% of conjugates with CD48-CD22 CHOs was for CD2 to accumulate in one or more clusters in the periphery of the IS (Fig. 5*D*). Similar results were obtained at 1 μM MCC peptide (data not shown).

CD2 and TCR; Co-localization Persists Despite CD48 Elongation—We investigated the co-localization of TCR and CD2 in large clusters detectable by confocal microscopy with the hypothesis that large clusters may act as sites in which TCR molecules are sequestered and prevented from participating in microcluster formation. Conjugates were prepared by incubat-

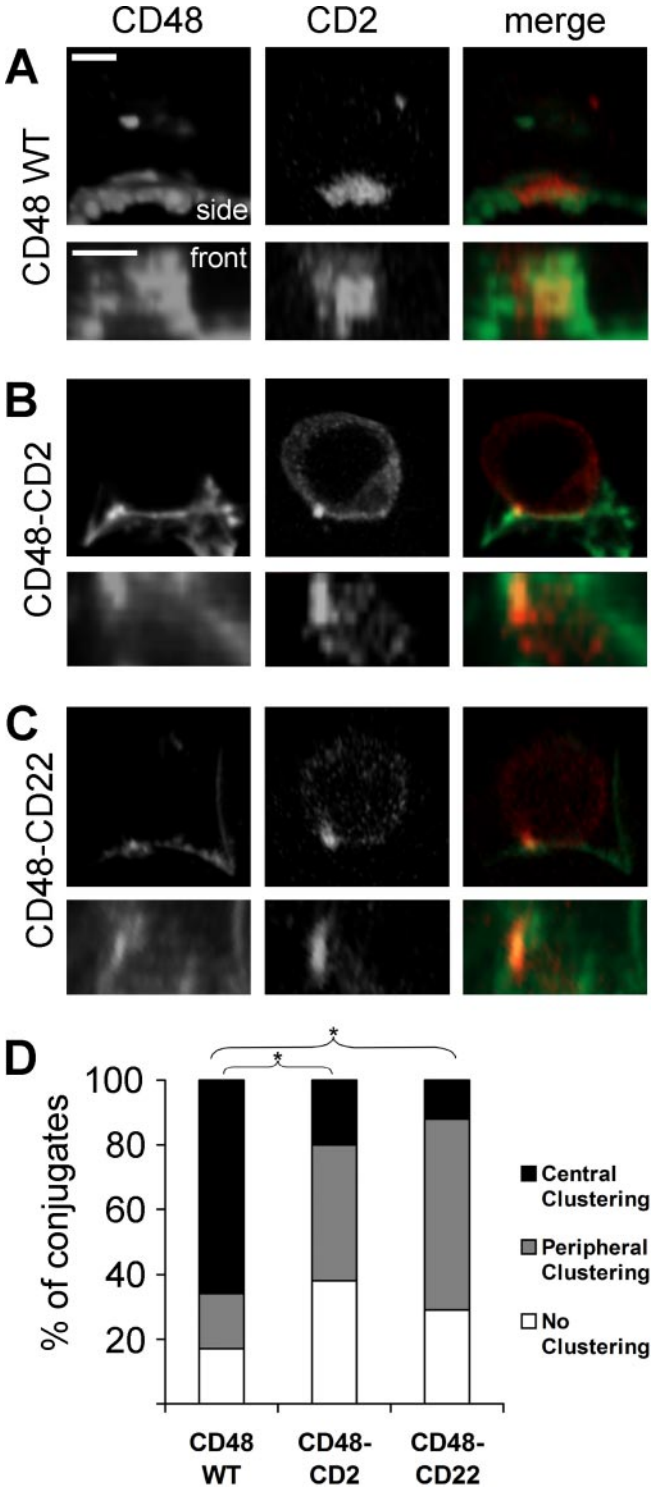

FIGURE 5. **CD2 is excluded from the cSMAC by elongated CD48.** *A–C*, representative *images* of 5C.C7 T cells conjugated to I-E^{k+} CHO APCs transfected with CD48-WT (*A*), CD48-CD2 (*B*), or CD48-CD22 (*C*). T cells were incubated for 30 min at 37 °C with the different CHO transfectants in the presence of 10 μM MCC 88–103. Cells were washed, fixed, and stained. CD2 appears in *red* and CD48 in *green* in the *merged image*. *Side* and *front* (*en face*) *views* are displayed. *Images* shown are of cells cultured with 10 μM MCC 88–103. *Scale bar*, 2 μm. *D*, quantification of the accumulation patterns of CD2 in T cells conjugated with the different CHO APCs. Cells were prepared as in *A*. Conjugated T cells displaying CD2 clusters in the center of the contact area were scored as having "central clustering" (■). Those displaying CD2 clusters solely outside of the center of the contact area were scored as having "peripheral clustering" (■). Conjugated T cells displaying no CD2 clusters at all were scored as having "no clustering" (□). All conjugated T cells were evaluated regardless of pattern, extent or presence of accumulation. Shown is the mean of three experiments. *, the differences in CD2 central clustering between T cells conjugated to CD48-WT CHO cells (n = 96) and T cells conjugated to CD48-CD2 (n = 74) or CD48-CD22 (n = 67) CHO cells are statistically significant, with $p < 0.0001$.

ing naive 5C.C7 T cells with the different I-E^k CHO cell transfectants in the presence of 10 μM MCC peptide. After 30 min, cells were washed and fixed, and the surface was stained for CD2 and TCR. Preparations were imaged by three-dimensional confocal microscopy as in Fig. 5. Only conjugates displaying both CD2 and TCR accumulations were analyzed. Both the central and peripheral CD2 clustering patterns were evaluated with regard to TCR co-localization. We did not observe consistent clustering of CD2 in ISs formed by CD48-negative I-E^k CHO cells pulsed with antigenic peptides (Fig. 6*A*). When CD2 clusters were observed, they were randomly distributed on the cell surface, and most were outside the contact area. This contrasts with the rapid signaling-dependent but ligand-independent clustering of CD2 with TCR in human T cells (23, 24). When CD48-WT was expressed in CHO cells, 92% of conjugates exhibited central CD2 clustering. This was a slightly higher percentage than noted in Fig. 5*D*, because the requirement for a detectable TCR cluster eliminated some cells that also lacked central CD2 clusters from consideration. TCR co-localized with CD2 in 100% of the IS with central CD2 clustering (Fig. 6*B*). In the few conjugates in which CD2 was found in the periphery (8%), no co-localization with TCR was detected (Fig. 6*B*). The pattern of CD2 clustering was different for IS with CHO cells expressing CD48-CD2 or CD48-CD22 with a 4:1 bias toward formation of CD2 clusters at one edge of the IS (Fig. 6, *C* and *D*). TCR co-localized with these peripheral CD2 clusters in 76% (CD48-CD2) or 65% (CD48-CD22) of synapses displaying this phenotype. This strong co-localization of TCR with CD2 in the periphery of the IS was reflected in less overall TCR clustering in the cSMAC among T cells engaging elongated CD48 forms (Fig. 6*E*). However, in 29% (CD48-CD2) and 18% (CD48-CD22) of synapses that exhibited co-localization of TCR with CD2 in a large co-cluster in the periphery, a diminished solitary TCR cluster was present in the cSMAC. Similar results were obtained at 1 μM MCC peptide (data not shown). Thus, TCR association with CD2 is maintained despite the latter's presence in the periphery when elongated CD48 forms are used. This is significant, since sequestering TCR in an area where it may have impaired interaction with MHCp complexes would naturally decrease the sensitivity of T cell activation.

DISCUSSION

We performed experiments with supported planar bilayers and imaging of T cell-APC IS in order to understand the basic rule of adhesion molecule segregation by size and how these relate to functional T cell activation. First, we have found that for the CD2 family adhesion molecules, increasing the size of the ligands by two or three Ig-like domains decreased adhesion efficiency by 10-fold, which was not expected. Second, we found that ligands of different sizes either interfere with each other or, if the difference in intermembrane spacing is sufficient (>2 nm), can form segregated adhesion domains in the same contact area. Third, we found that in the mixed contact areas,

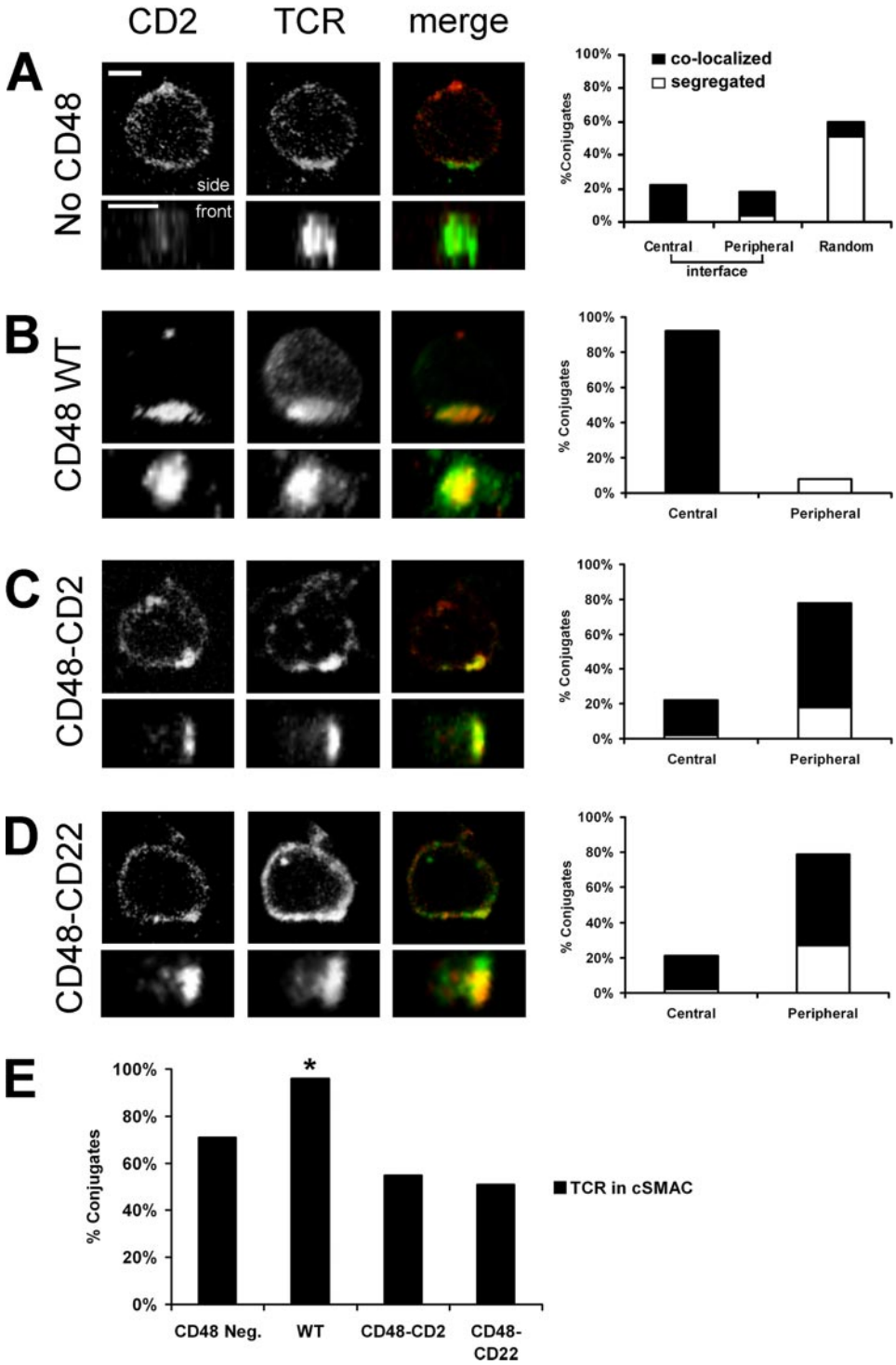

FIGURE 6. **Sequestration of the TCR in peripheral clusters induced by elongated CD48s.** *A–D*, *images* and quantification of 5C.C7 T cells conjugated to I-E^{k+} CHO APCs transfected with CD48 null (*A*) CD48-WT (*B*), CD48-CD2 (*C*), or CD48-CD22 (*D*). *Images* and cells were prepared as described in the legend to Fig. 5. CD2 appears in *red*, and TCR is shown in *green* in the *merged images*. *Side* and *front* (*en face*) *views* are shown. *Scale bar*, 2 μm. Conjugates were scored both for the CD2 pattern of accumulation and for the occurrence of TCR co-localization with it. Conjugates were scored "central" when CD2 accumulated in the central area of contact. They were scored "peripheral" when CD2 accumulated solely outside of the central area of contact. T cells conjugated to CD48-negative APCs had an irregular CD2 distribution that was scored as "central" or "peripheral" only when it accumulated in the interface area. When it did not, conjugates were scored as having "random" CD2 distribution. Regarding co-localization with TCR, conjugates were scored "co-localized" (■) when T cells displayed at least a partial overlap of CD2 and TCR. They were scored "segregated" (□) when no co-localization of CD2 and TCR was evident. Only conjugates displaying both CD2 and TCR clusters were scored. Shown is the mean of three experiments. *E*, TCR presence in the cSMAC area. Conjugates were evaluated for the presence of TCR in the central area of contact. Only conjugated T cells co-expressing CD2 clusters were evaluated. Shown is the mean of three experiments. *, the differences in TCR central clustering between T cells conjugated to CD48-WT CHO cells ($n = 76$) and T cells conjugated to CD48-CD2 ($n = 56$), CD48-CD22 ($n = 50$) or CD48 null CHO cells ($n = 46$) are significant, with $p < 0.05$.

small molecules suffer greater impairment than larger molecules, even when the larger molecules are otherwise less efficient in mediating adhesion. Fourth, we found that interaction of CD2 with elongated CD48 resulted in a dramatic disorgani-

zation of the immunological synapse with formation of an ectopic adhesion/TCR domain correlated with decreased sensitivity to antigen.

It has been proposed that extending the reach of small adhesion molecules like CD2/CD58 could increase their interactions by extending them above the glycocalyx (3). However, it was found that adding four Ig-like domains to the human CD2 ligand CD58 provided an advantage at 4 °C but was neutral for adhesion at 24 or 37 °C in a cell-cell system in the absence of antigen (34). Here we have used supported planar bilayers, in which CD2/CD48 interactions self-assemble a highly ordered contact area (27). To our surprise, we found that extending CD48 by two or three domains increases the density of CD48 needed to mediate adhesion by 10-fold at equilibrium. We did not determine the two-dimensional K_d, because we did not have the appropriate control proteins to accurately estimate the exclusion of free extended forms of CD48 from the contact areas. However, the requirement for a 10-fold higher density of extended CD48 forms to mediate adhesion is consistent with a 10-fold higher two-dimensional K_d. The CHO cells express high enough levels of the extended CD48 forms to saturate the adhesion response; thus, this difference in activity between CD48-WT and extended forms was missed previously.

Our electron microscopy tomography results are fully consistent with prior results that adding Ig-like domains increases intermembrane spacing by ~1 nm per domain added (26). This suggests that added Ig-like domains are not rigid and allow bending (see schematics in Fig. 7). The variation in intermembrane spacing was similar between all ligands, consistent with all three ligands self-assembling a highly ordered contact area (27). We can envision that the more flexible extended CD48 molecules have two disadvantages compared with CD48-WT. One is that the CD2 binding site of CD48 may need to search a larger volume for ligands, which will decrease the on rate for the two-dimensional binding reaction. Another factor in controlling the two-dimensional binding reaction is the entropy loss on receptor-ligand binding. The entropy loss will be greater for more flexible molecules, and this adds +0.5 kcal/mol per degree of freedom lost to the ΔG of the binding reaction. The CD2-CD48WT interaction spans an intermembrane distance predicted by crystallographic data of 13.4 nm (17, 18). Relatively small, heavily glycosylated molecules like CD2 and CD48 may also have this extended conformation in the unbound state. It is probable that the CD2-CD48, CD28-B7, and TCR-MHCp interactions exist near an optimal balance point between the steric costs of close approach between cells and minimizing the search volume and entropy loss during formation of a highly ordered contact area.

We have used the supported planar bilayer system to visualize distribution of topologically distinct ligands competing for the same receptors. Utilization of the same receptor does not eliminate potential cytoskeletal contributions, but it does equalize them and makes it much less likely that differential cytoskeletal interactions would be a basis for segregation. Our results reveal two mechanisms by which topologically distinct ligands influence each other in a contact area. Fig. 7 presents a hypothetical phase diagram of the type introduced by Goldstein and colleagues to discuss segregation in IS formation (35). This

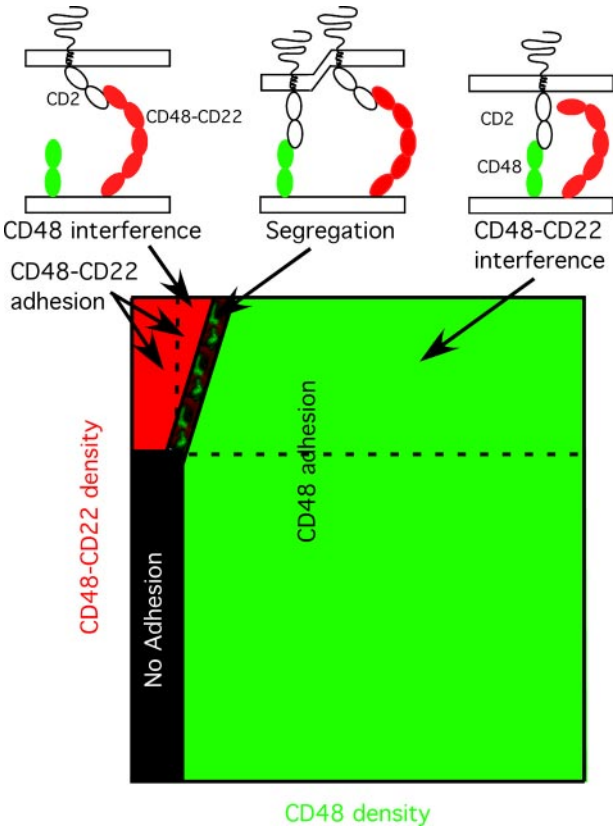

FIGURE 7. **Phase diagram for CD2 mediated adhesion to mixtures of CD48-WT and CD48-CD22 based on results of this study.** The *axes* are based on relative linear concentrations of CD48-WT (*green*) and CD48-CD22 (*red*) with *colors* reflecting the dominant interaction. The *black areas* have no adhesion, and segregated patterns are obtained in a narrow range as indicated. The molecular *schematic diagrams* reflect our supposition that the CD48-CD22 is flexible, but this is not necessary, since bending only at the tethering point to the membrane could achieve the same effect.

simplified schematic treats adhesion mediated by CD2 to CD48-WT or CD2 to CD48-CD22 interactions as yes or no phenomena with thresholds that are 10-fold lower for CD48-WT than for CD48-CD2 or CD48-CD22. Different areas on the phase diagram correspond to areas in which only CD48-WT or CD48-CD22 contribute to adhesion. When both molecules are above the threshold for mediating adhesion, they can either interfere with each other to generate single component contacts or as the CD48-WT/CD48-CD22 ratio approaches 1:9, the possibility of coexisting segregated domains is greater. Formation of mixed contacts in which TCR and LFA-1 microclusters segregate is more tolerant to variation in the ratio of TCR to LFA-1 than the observed formation of mixed contacts in which CD2 molecules are bound to ligands of different size (11). This is probably related to the active F-actin-dependent processes involved in forming integrin and TCR microclusters (12, 13, 36, 37).

Our experiments provide new insight into the mechanism by which elongated forms of CD48 suppress T cell antigen recognition (25). We can put our observations in the context of current models for T cell signaling in microclusters (11–14). In this model TCRs exist in three states: 1) presignaling TCRs that are in small unstable clusters or single receptors in the periphery, 2) TCRs that engage MHCp and form microclusters that signal for

~1–2 min, and 3) TCRs in macroclusters in the cSMAC that are in a postsignaling phase until degradation or recycling. We propose that CD2 interactions with the elongated CD48 take some of the TCR in state 1, the presignaling state, and prevent them from participating in forming state 2, the signaling microclusters. The idea that the CD48 mutants act presignaling is consistent with earlier data (25) and builds on our existing model for signaling dynamics during T cell activation. Since CD2 associates with the TCR on the surface of T cells (21, 38), the impact of CD2 binding to CD48-CD2 or CD48-CD22 is profound, since it forces the TCR into adhesion domains that have too large an intermembrane separation for TCR to interact with MHCp. This can be partially overcome by increasing the MHCp density, because this allows the T cell to use the lower density of free TCR outside the CD2 clusters. A question that remains is why the CD2-extended CD48 interactions are focused in a single eccentric cluster rather than being distributed throughout the periphery. The CD2-extended CD48 interactions will be most stable in micrometer scale self-assembled domains. We have recently found that contractile oscillations in the distal supramolecular activation complex lead to lateral waves that circle the outside of the IS and may lead to circumferential transport of self-assembled CD2 clusters formed with extended ligands, which then coalesce into a single large cluster (10, 39).

In summary, we have shown here that in contacts mediated by the same receptor, the size of the ligand determines the intermembrane gap, the adhesion strength of the receptor-ligand interaction, and the spatial localization of the interaction in the contact area. Importantly, we have shown that elongated receptor-ligand pairs segregate from wild type ones, induce abnormalities in IS formation, and inhibit T cell activation, demonstrating for the first time molecular segregation purely by size and the consequence of this principle when hyperextended receptor-ligand pairs are used.

Acknowledgments—We thank M. Davis, R. Varma, and G. Shakhar for reagents and advice. We utilized the facilities of the New York Structural Biology Center, which is a STAR center supported by the New York State Office of Science, Technology, and Academic Research.

REFERENCES

1. Garcia, K. C., Degano, M., Stanfield, R. L., Brunmark, A., Jackson, M. R., Peterson, P. A., Teyton, L., and Wilson, I. A. (1996) *Science* **274,** 209–219
2. Dustin, M. L., Bromley, S. K., Davis, M. M., and Zhu, C. (2001) *Annu. Rev. Cell Dev. Biol.* **17,** 133–157
3. Springer, T. A. (1990) *Nature* **346,** 425–434
4. Weiss, A., and Littman, D. R. (1994) *Cell* **76,** 263–274
5. Kato, K., Koyanagi, M., Okada, H., Takanashi, T., Wong, Y. W., Williams, A. F., Okumura, K., and Yagita, H. (1992) *J. Exp. Med.* **176,** 1241–1249
6. Monks, C. R., Freiberg, B. A., Kupfer, H., Sciaky, N., and Kupfer, A. (1998) *Nature* **395,** 82–86
7. Dustin, M. L., Olszowy, M. W., Holdorf, A. D., Li, J., Bromley, S., Desai, N., Widder, P., Rosenberger, F., van der Merwe, P. A., Allen, P. M., and Shaw, A. S. (1998) *Cell* **94,** 667–677
8. Grakoui, A., Bromley, S. K., Sumen, C., Davis, M. M., Shaw, A. S., Allen, P. M., and Dustin, M. L. (1999) *Science* **285,** 221–227
9. Freiberg, B. A., Kupfer, H., Maslanik, W., Delli, J., Kappler, J., Zaller, D. M., and Kupfer, A. (2002) *Nat. Immunol.* **3,** 911–917
10. Sims, T. N., Soos, T. J., Xenias, H. S., Dubin-Thaler, B., Hofman, J. M., Waite, J. C., Cameron, T. O., Thomas, V. K., Varma, R., Wiggins, C. H., Sheetz, M. P., Littman, D. R., and Dustin, M. L. (2007) *Cell* **129,** 773–785
11. Varma, R., Campi, G., Yokosuka, T., Saito, T., and Dustin, M. L. (2006) *Immunity* **25,** 117–127
12. Kaizuka, Y., Douglass, A. D., Varma, R., Dustin, M. L., and Vale, R. D. (2007) *Proc. Natl. Acad. Sci. U. S. A.* **51,** 20296–20301
13. Campi, G., Varma, R., and Dustin, M. L. (2005) *J. Exp. Med.* **202,** 1031–1036
14. Yokosuka, T., Sakata-Sogawa, K., Kobayashi, W., Hiroshima, M., Hashimoto-Tane, A., Tokunaga, M., Dustin, M. L., and Saito, T. (2005) *Nat. Immunol.* **6,** 1253–1262
15. Takagi, J., Petre, B. M., Walz, T., and Springer, T. A. (2002) *Cell* **110,** 599–611
16. Staunton, D. E., Marlin, S. D., Stratowa, C., Dustin, M. L., and Springer, T. A. (1988) *Cell* **52,** 925–933
17. van der Merwe, P. A., McNamee, P. N., Davies, E. A., Barclay, A. N., and Davis, S. J. (1995) *Curr. Biol.* **5,** 74–84
18. Wang, J. H., Smolyar, A., Tan, K., Liu, J. H., Kim, M., Sun, Z. Y., Wagner, G., and Reinherz, E. L. (1999) *Cell* **97,** 791–803
19. He, W., Cowin, P., and Stokes, D. L. (2003) *Science* **302,** 109–113
20. Al-Amoudi, A., Diez, D. C., Betts, M. J., and Frangakis, A. S. (2007) *Nature* **450,** 832–837
21. Bockenstedt, L. K., Goldsmith, M. A., Dustin, M., Olive, D., Springer, T. A., and Weiss, A. (1988) *J. Immunol.* **141,** 1904–1911
22. Holdorf, A. D., Green, J. M., Levin, S. D., Denny, M. F., Straus, D. B., Link, V., Changelian, P. S., Allen, P. M., and Shaw, A. S. (1999) *J. Exp. Med.* **190,** 375–384
23. Douglass, A. D., and Vale, R. D. (2005) *Cell* **121,** 937–950
24. Faroudi, M., Zaru, R., Paulet, P., Muller, S., and Valitutti, S. (2003) *J. Immunol.* **171,** 1128–1132
25. Wild, M. K., Cambiaggi, A., Brown, M. H., Davies, E. A., Ohno, H., Saito, T., and van der Merwe, P. A. (1999) *J. Exp. Med.* **190,** 31–41
26. Choudhuri, K., Wiseman, D., Brown, M. H., Gould, K., and van der Merwe, P. A. (2005) *Nature* **436,** 578–582
27. Dustin, M. L., Golan, D. E., Zhu, D. M., Miller, J. M., Meier, W., Davies, E. A., and van der Merwe, P. A. (1997) *J. Biol. Chem.* **272,** 30889–30898
28. Tseng, S. Y., Liu, M., and Dustin, M. L. (2005) *J. Immunol.* **175,** 7829–7836
29. Carpen, O., Dustin, M. L., Springer, T. A., Swafford, J. A., Beckett, L. A., and Caulfield, J. P. (1991) *J. Cell Biol.* **115,** 861–871
30. Winkler, H., and Taylor, K. A. (2006) *Ultramicroscopy* **106,** 240–254
31. Gaglia, J. L., Mattoo, A., Greenfield, E. A., Freeman, G. J., and Kuchroo, V. K. (2001) *Cell. Immunol.* **213,** 83–93
32. Dustin, M. L., Starr, T., Varma, R., and Thomas, V. K. (2007) in *Current Protocols in Immunology* (Coligan, J. E., Bierer, B. E., Margulies, D. H., Shevach, E. M., and Strober, W., eds) John Wiley and Sons, Inc., New York
33. Leupin, O., Zaru, R., Laroche, T., Muller, S., and Valitutti, S. (2000) *Curr. Biol.* **10,** 277–280
34. Chan, P. Y., and Springer, T. A. (1992) *Mol. Biol. Cell* **3,** 157–166
35. Coombs, D., Dembo, M., Wofsy, C., and Goldstein, B. (2004) *Biophys. J.* **86,** 1408–1423
36. Calderwood, D. A., and Ginsberg, M. H. (2003) *Nat. Cell Biol.* **5,** 694–697
37. Tadokoro, S., Shattil, S. J., Eto, K., Tai, V., Liddington, R. C., De Pereda, J. M., Ginsberg, M. H., and Calderwood, D. A. (2003) *Science* **302,** 103–106
38. Brown, M. H., Cantrell, D. A., Brattsand, G., Crumpton, M. J., and Gullberg, M. (1989) *Nature* **339,** 551–553
39. Dobereiner, H.-G., Dubin-Thaler, B., Hofman, J., Xenias, H. S., Sims, T. N., Giannone, G., Dustin, M. L., Wiggins, C., and Sheetz, M. P. (2006) *Phys. Rev. Lett.* **97,** 381021–381024